analytical chemistry

Article

pubs.acs.org/ac

Graphene Oxide-Assisted Nucleic Acids Assays Using Conjugated Polyelectrolytes-Based Fluorescent Signal Transduction

Fan Li,[‖,†] Jie Chao,[‡,†] Zhenhua Li,[‖] Shu Xing,[‖] Shao Su,[‡] Xiaoxia Li,[‖] Shiping Song,[‖] Xiaolei Zuo,[‖] Chunhai Fan,[‖] Bin Liu,[§] Wei Huang,[‡] Lianhui Wang,[‡] and Lihua Wang*[,‖]

[‖]Division of Physical Biology and Bioimaging Center, Shanghai Synchrotron Radiation Facility, Shanghai Institute of Applied Physics, Chinese Academy of Sciences, Shanghai 201800, China

[‡]Key Laboratory for Organic Electronics and Information Displays (KLOEID), Institute of Advanced Materials (IAM), School of Materials Science and Engineering, Nanjing University of Posts and Telecommunications, Nanjing, Jiangsu 210023, China

[§]Department of Chemical and Bimolecular Engineering, National University of Singapore, 117576, Singapore

Supporting Information

ABSTRACT: In this work, we investigated the interactions between graphene oxide (GO) and conjugated polyelectrolytes (CPEs) with different backbone and side chain structures. By studying the mechanism of fluorescence quenching of CPEs by GO, we find that the charge and the molecular structure of CPEs play important roles for GO−CPEs interactions. Among them, electrostatic interaction, $\pi-\pi$ interaction, and cation$-\pi$ bonding are dominant driving forces. By using a cationic **P2**, we have developed a sensitive homogeneous sensor for DNA and RNA detection with a detection limit of 50 pM DNA and RNA, which increased the sensitivity by 40-fold as compared to GO-free CPE-based sensors. This GO-assisted CPE sensing strategy is also generic and shows a high potential for biosensor designs based on aptamers, proteins, peptides, and other biological probes.

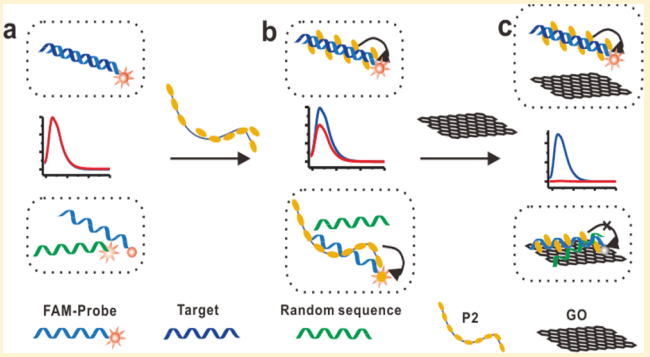

Water-soluble, fluorescent π-conjugated polyelectrolytes (CPEs) provide a unique signal-amplification platform for the development of highly sensitive fluorescence-based sensors.[1−4] As a high-efficiency "antenna" that channels excitation energy to the reporter fluorophore, the CPEs amplified the fluorescence signal by orders of magnitude.[5] On the basis of the significant signal amplification, several groups have recently developed sensitive sensors for biologically relevant and clinically important targets including proteins, DNA, carbohydrates, and ions.[2,6−13] However, most of these CPE-based sensors depends on the nonspecific electrostatic interaction of CPEs and biomolecules. The presence of charged nonspecific molecules often results in the high background signal and false positive results, which leads to the poor sensitivity and selectivity.[7,9,14,15]

Graphene oxide (GO) provides possibilities to improve the fluorescence biosensors based on its superquenching ability to fluoresce and characteristic interaction with CPEs. Thus, the GO−CPEs hybrid system has been employed as an efficient biosensing platform for the detection of protein, DNA, and other small molecules.[16−21] Whereas various studies employed GO to improve the performance of fluorescence sensors through lowering the background noise, it remains unclear how GO interacts with CPEs. Here, we investigated the interactions between GO and various CPEs possessing different structures and charges. On the basis of the understanding of the GO−CPEs hybrid system, we developed a biosensing system to detect DNA and RNA targets with high sensitivity and selectivity.

EXPERIMENTAL SECTION

Materials. Graphite powder was purchased from China National Pharmaceutical Group Corporation. All other chemicals were of analytical grade. All chemicals were used without further purification. Milli Q Water was used for the whole procedure. The fluorescent CPEs were synthesized as previously reported.[19] GO was prepared according to our previous report and characterized with a tapping-mode atomic force microscope (AFM) (Figure S1, Supporting Information). DNA oligonucleotides were synthesized and purified by HPLC (Sangon Biotechnology Inc., Shanghai). The sequences of the involved oligonucleotides are listed in Table 1.

Fluorescence Assays. Fluorescence spectra were measured on a fluorometer (Hitachi F-4500 Fluorescence spectrophotometer). In the CPEs fluorescence quenching assay, 10 μL of GO solution (1 mg/mL) was added into 1 mL of the different CPEs buffer (100 mM NaCl, 10 mM PB, pH 7.4). The

Received: December 15, 2014
Accepted: March 4, 2015
Published: March 4, 2015

DOI: 10.1021/ac504658a
Anal. Chem. 2015, 87, 3877−3883

Table 1. Sequences of Oligonucleotides

	sequences
ssDNA1	5′-FAM-TCG TTG GAG TTT GTC TG-3′
T (target)	5′-CAG ACA AA**C** TCC AAC GA-3′
R (random sequence)	5′-GCA GAG CCA GTT CCA AG-3′
M1 (mismatch-T)	5′-CAG ACA AA**T** TCC AAC GA-3′
M2 (mismatch-A)	5′-CAG ACA AA**A** TCC AAC GA-3′
M3 (mismatch-G)	5′-CAG ACA AA**G** TCC AAC GA-3′
ssDNA2	5′-FAM-CCA TCT TTA CCA GAC AGT GTT A-3′
miR141	5′-UAA CAC UGU CUG GUA AAG AUG G-3′

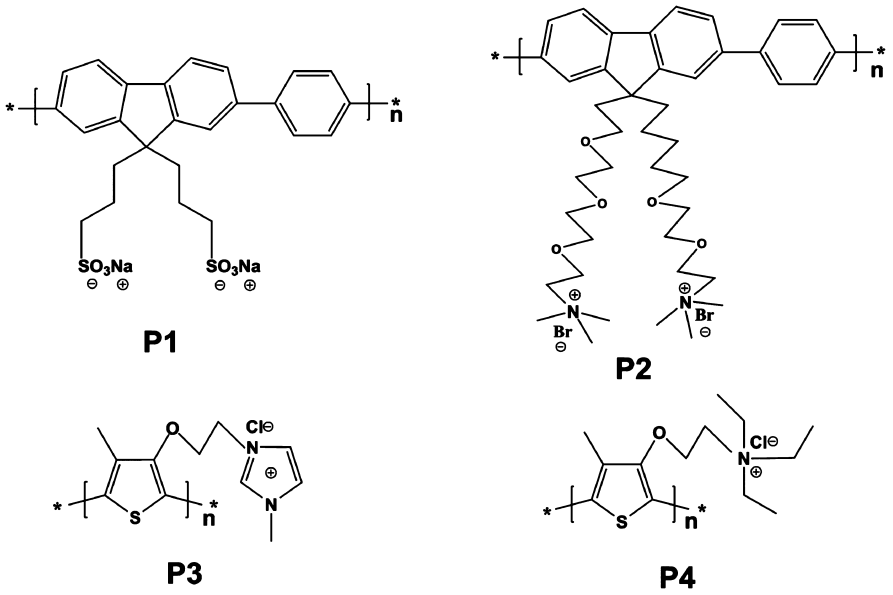

Figure 1. Molecular structures of CPEs.

fluorescence spectra were recorded after GO was added with the excitation and emission wavelengths as noted (**P1** Ex: 374 nm, Em: 384−700 nm; **P2** Ex: 376 nm, Em: 386−700 nm; **P3** Ex: 415 nm, Em: 425−700 nm; **P4** Ex: 382 nm, Em: 392−700 nm).

In optimizing concentrations of **P2**, the fluorescent probe (**ssDNA1**, 40 nM) was hybridized with the target sequence (**T**, 40 nM) in 0.5 mL of PBS buffer (100 mM NaCl, 10 mM PB, pH 7.4) for 10 min at 37 °C. In the FRET assay, 0.5 mL of the PBS buffer was mixed with different volumes (10, 20, 30, 40, 50, and 60 μL) of **P2** solution (10^{-4} M), and the final assay volumes were 1 mL with the addition of different volumes of buffer for every assay group. The fluorescence spectra were recorded after **P2** was added with excitation and emission wavelength of 376 nm and 386−700 nm, respectively.

In the fluorescence assays with **P2** and GO, the fluorescent probes (**ssDNA1**, 20 nM) were hybridized with the target sequence (**T**, 20 nM) or random sequence (**R**, 20 nM) in PBS buffer for 10 min at 37 °C, and then, 10 μL of GO solution (1 mg/mL) was added into 1 mL of the mixture of the PBS buffer with **P2**.

For the quantitative assay, different concentrations of **T** (0, 0.2, 0.5, 1, 2, 5, 10, 20, and 40 nM) were investigated. For the SNP assay, three different SNP sequences (**M1**, **M2**, **M3**, 20 nM) were employed. All experiments were performed with the same procedures as above.

In the miR141 quantitative assay, the fluorescent probes (**ssDNA2**, 20 nM) were hybridized with the different concentrations of miR141 (0, 0.05, 0.1, 1, 5, 10, 20, and 50 nM) for 10 min at 37 °C. Then, 10 μL of GO solution (1 mg/mL) was added into 1 mL of the mixture of the PBS buffer with **P2**. In the simulated detection assay of miR141, the total RNA extraction sample (82.8 ng/mL) was used as a control, and the mixed sample of total RNA and miR141 was also determined.

RESULTS AND DISCUSSION

Here, we prepared four CPEs with different charges, backbones, and side chain structures to investigate the interaction between GO and CPEs (Figure 1).[22−26] Two poly(fluorine-*co*-phenylene) (**PFP**) derivatives and two poly(thiophene) (**PT**) derivatives are used here, including poly(9,9-bis(4′-sulfonatobutyl) fluorine-*co*-*alt*-1,4-phenylene) sodium salt (PFS, **P1**), poly(2,2′-(2,2′-(2,2′-(2,2′-(2-phenyl-9*H*-fluorine-9,9-diyl)bis-(ethane-2,1-diyl))bis(oxy)bis(ethane-2,1-diyl))bis(oxy)bis(ethane-2,1-diyl))bis(oxy)bis(*N*,*N*-trimethylethanammonium) bromide) (**P2**), poly(1*H*-imidazolium-1-methyl-3-{2-[(4-methyl-3-thienyl)-oxy]ethyl}chloride) (**P3**), and poly [3-(3′-*N*,*N*,*N*-triethylamino-1′-ethyloxy)-4-methyl-2,5-thiophene hydrochloride] (**P4**). In which, the charge, the structure of backbones, and side chains are varied. The charge of **P1** is different from the other three polymers; in detail, **P1** has two negative charges at its side chain per unit, while **P2** has two positive charges, and **P3** and **P4** have one positive charge. For backbone chain structures of these four polymers, the backbones of **P1** and **P2** are fluorine-*co*-phenylene, while **P3** and **P4** are thiophene. Generally, the conjugation extent of PFP is higher than that of

DOI: 10.1021/ac504658a
Anal. Chem. 2015, 87, 3877−3883

PT because of more aromatic rings in PFP than that of PT (3 vs 1). For positive **P3** and **P4** with PT unit, their side chain structures are different. The imidazolium group in **P3** exhibited a higher conjugation degree than the alkyl group in **P4**, we believe these differences will result in different interactions with GO.

We first determined the fluorescence characters of these four polymers, and Figure 2 exhibited their characteristic fluorescence emission spectra (black line). With the same concentration (20 nM), the PFP derivatives exhibited much higher fluorescence intensity than PT ones (882/**P1**, 732/**P2** vs 204/**P3**, 27/**P4**), implying PFP was more suitable than PT to develop a good fluorescent biosensor. Furthermore, we mixed these four CPEs and GO to investigate the fluorescence quenching capability of GO to CPEs. We observed that the fluorescence of **P1** (20 nM) was slightly quenched (31.9%) by 10 μg/mL of GO, which indicated the relatively weak interaction between **P1** and GO. We reason that the negatively charged oxygen-containing functional groups on GO repulsed the negatively charged **P1** because of the electrostatic repulsion, which decreased the binding force between GO and **P1**. To prove our hypothesis, we mixed GO and the other three CPEs (**P2**, **P3**, and **P4**) with positive charges. As expected, we observed that the fluorescence of these three CPEs were almost totally quenched by GO, which indicated that the electrostatic adsorption contributed to the interaction between GO and positively charged CPEs. Further quantitative analysis demonstrated that the quenching efficiency for **P2**, **P3**, and **P4** was 99%, 99.3% and 94.3%, respectively. We also found that the fluorescence quenching was a quick process, and the fluorescence of all four polymers could be quenched in less than 1 min (Figure S2, Supporting Information). The fast quenching kinetics greatly facilitated the rapid detection in various fields.

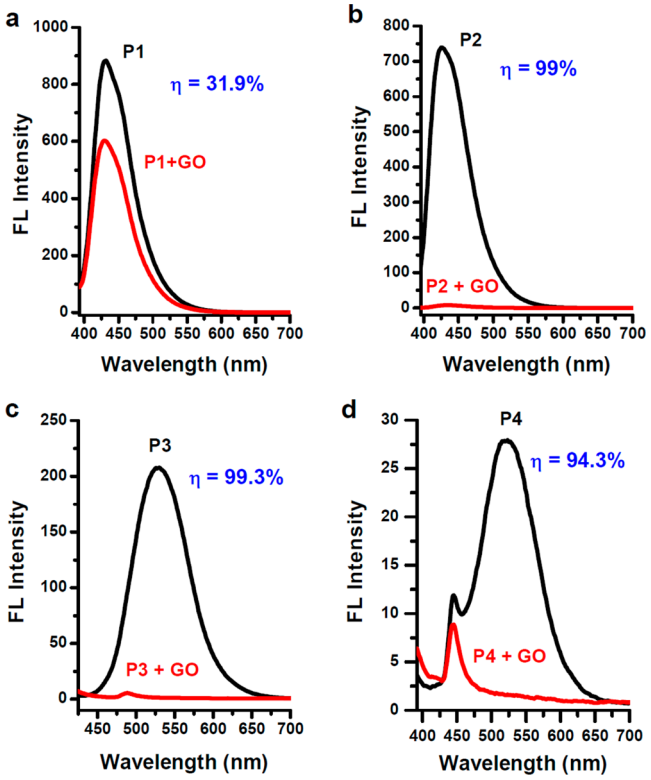

Figure 2. Typical fluorescence spectra of four CPEs (20 nM) in the absence and presence of GO (10 μg/mL).

As previously reported, GO is a graphene sheet decorated with an epoxide and hydroxyl group on the basal plane as major components along with carbonyl and carboxyl groups on the edges as minor components. The presence of ionic groups and an aromatic domain suggests that GO can interact with molecules in a number of ways[16,17,27−29] Ionic groups such as −OH and −COOH that decorate the planes and edges allow electrostatic interaction with charged molecules. Therefore, the electrostatic repulsion forced the negatively charged **P1** apart from GO, which resulted in the weak interaction between them and the low fluorescence quenching efficiency. Meanwhile, positive polymers can be easily adsorbed on GO with high affinity, which resulted in high fluorescence quenching of **P2**, **P3**, and **P4**. In comparison with the other three positively charged polymers, the highest fluorescence quenching efficiency arising from the negatively charged **P1** implied the electrostatic interaction dominantly contributed to the tight GO−CPEs binding. The electrostatic interaction between CPEs and GO was further proved by determining the fluorescence change of GO−**P2** in various buffers with different ion strengths. Figure S3, Supporting Information, demonstrated that the fluorescence intensity of **P2** declined along with the increase of ion strength, which coincided with the behavior of the GO−DNA interaction,[30−32] indicating that the electrostatic interaction greatly influenced the GO−**P2** interaction.[33]

The aromatic compounds can easily adsorb on GO because of the strong $\pi-\pi$ stacking interaction between the ring structures and the hexagonal cells of the graphene.[17,34,35] Here, we investigated the influence of backbone chain structure of CPE on the interaction of GO and CPEs. We observed that, although **P2** and **P3** possessed different backbone chains, their fluorescence was efficiently quenched (99% for **P2** and 99.3% for **P3**). Therefore, we concluded that the backbone chain of CPEs containing highly conjugated ring structures allowed a similar strong $\pi-\pi$ interaction of GO and CPEs. In addition, the structure of the side chain may also influence the GO−CPEs interaction. We found that the quenching efficiency of GO to **P4** (94.3%) was slightly lower than that to **P3** (99.3%). Since they have the same structure of backbone chain, this slight difference may probably originate from the $\pi-\pi$ interaction of the methylmidazole groups and GO. In order to understand the characteristic $\pi-\pi$ interaction between them, various organic solvents with different polarity were added into PBS. Here, we employed DMSO, NMP, ethanol, and THF whose polarity indices were 7.2, 6.7, 5.2, and 4.0, respectively,[36,37] while the polarity index of water was 9.0. The fluorescence of **P2** in 5:5 PBS buffer/organic solvent was determined and presented in Figure S4, Supporting Information. The fluorescence of **P2** in DMSO was the lowest, demonstrating that **P2** adsorbed on GO in DMSO with high affinity. The fluorescence intensity of **P2** followed the order of THF, ethanol, NMP, and DMSO, which coincided with their polarity indices. That means the lower the polarity index, the lower is the GO−**P2** interaction, implying that the GO−**P2** interaction can be regulated by solvent through the influence of the $\pi-\pi$ interaction.

The multiplex interactions between GO and CPEs allow their tight binding, and then, the superquenching ability of GO greatly contributes to the high efficiency of fluorescence quenching of CPEs. The formation of the GO−CPEs complex might lead to a "polymer ensemble" in which a GO sheet could

DOI: 10.1021/ac504658a
Anal. Chem. 2015, 87, 3877−3883

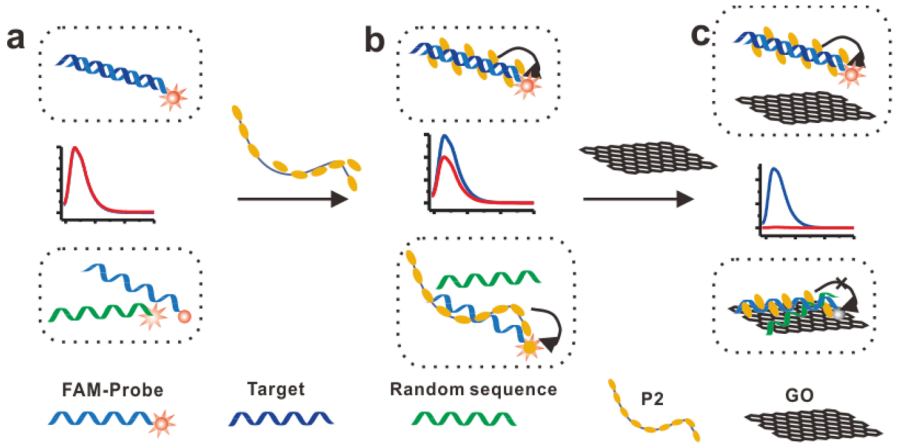

Figure 3. Schematic presentation of DNA analysis with the GO−CPEs hybrid system.

quench a large number of polymer chains. Due to the highly efficient and relatively long-range energy transfer, the quenching of CPEs by GO might be several orders of magnitude more efficient than any previously reported conjugated polymer−quencher pair, as well 9−10 orders of magnitude more efficient than typical small molecule dye−quencher pairs.[38]

On the basis of the extensive investigation of the interactions between CPEs and GO, here, we further designed novel CPEs-based strategies for DNA detection by combining GO. **P2** was chosen on account of its high fluorescence intensity and high fluorescence quenching efficiency by GO, and the high signal and low background implied GO−**P2** was an excellent biosensing system. A single stranded DNA (ssDNA) labeled with a 5′ fluorescein (FAM, fluorescein amidite, acceptor), 5′-FAM-TCG TTG GAG TTT GTC TG-3′ (**ssDNA1**), was employed to capture the DNA target (**T**, 5′-CAG ACA AAC TCC AAC GA-3′).

As Figure 3 illustrated, the hybridization of **ssDNA1** and **T** did not cause a fluorescence change of **ssDNA1**. After addition of **P2**, the fluorescence intensity significantly increased for the double stranded (dsDNA) in comparasion with **ssDNA1**. We deduced that the dsDNA with higher charge density can bind to the **P2** tightly, which brought the **P2** and FAM into close proximity for efficient fluorescence resonance energy transfer (FRET). Then, negatively charged GO was introduced to quench the background fluorescence signal from **ssDNA1** based on the adsorption between GO and ssDNA. In addition, GO also could quench the fluorescence of positively charged **P2** through its tight binding on the surface of GO. Therefore, the signal-to-noise ratio (S/N) could be improved greatly, which led to the improved sensitivity of the detection.

We first optimized the concentration of **P2** (1−6 μM, Figure 4a) in the presence of dsDNA to get the highest fluorescent signal. We observed that the fluorescence increased along with the increase of **P2** concentration, and the biggest increase happened at 3−4 μM. After addition of GO, the fluorescence of **P2**/dsDNA greatly changed with the increase of **P2** (Figure 4b). The fluorescence changes of **P2** in the absence and presence of GO were analyzed (Figure 4c), and the decrease of fluorescence intensity at 430 nm after addition of GO, ΔF_{430}, was employed to value the exhausted energy of **P2**, which increased along with the increase of **P2**, implying **P2** was excessive for GO. Meanwhile, the decrease of fluorescence intensity at 537 nm, ΔF_{537}, reached the highest at 4 μM,

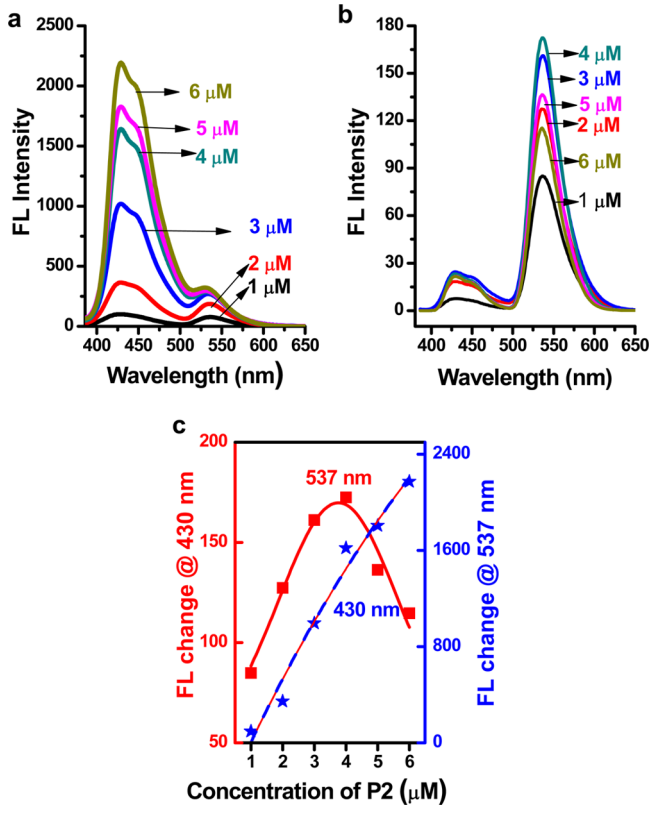

Figure 4. Fluorescence spectra of complexes of dsDNA with **P2** at different concentrations (1−6 μM) in the (a) absence and (b) presence of 10 μg/mL GO. (c) The fluorescence change of two characteristic peaks at 430 and 537 nm.

implying 3−4 μM of **P2** was suitable for the further DNA detection.

The performance of the **P2**-based sensor could be improved by adding GO, and the noise signal from other nontarget sequence could be inhibited efficiently. Here, 3 μM **P2** was used to avoid abundant polymers in the GO−**P2** hybridized probe for DNA detection. We investigated the selectivity of our sensor, in which a complete complementary DNA (**T**) and a random DNA (**R**) were employed. The ratio of fluorescence of target to that of random, F_T/F_R, was used to valuate the S/N ratio. Without GO, we obtained a signal change of 0.81 in the fluorescence ratio (Figure 5a). By using a newly designed

DOI: 10.1021/ac504658a
Anal. Chem. 2015, 87, 3877−3883

system with GO, we observed a signal change of 14.93, which was a significant improvement. The S/N ratio could be improved by up to 18-fold.

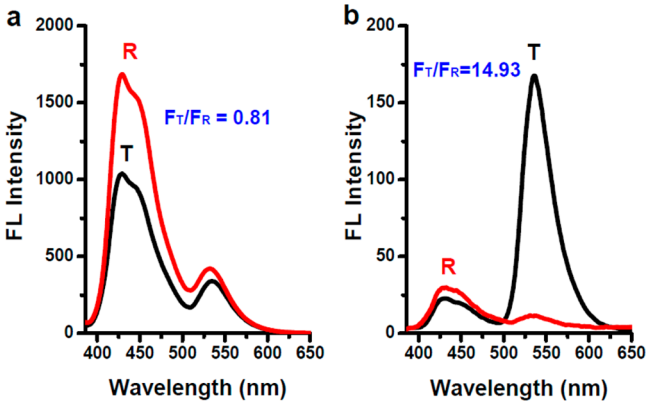

Figure 5. Fluorescence spectra of complexes of **ssDNA1/T** (double stand) and **ssDNA1/R** (single strand) with **P2** in the (a) absence and (b) presence of GO.

This GO−**P2** hybrid system-based DNA detection platform was then used for DNA detection (Figure 6). We first hybridized **ssDNA1** with target sequence at various concentrations for 10 min, and then, the mixtures were combined with **P2**. After that, the GO sheets were added. As shown in Figure 6a, we observed that the FRET signal of fluorescence at 537 nm was increased along with the increase of the target concentration. Our DNA sensor had a linear range of 0−20 nM, with a detection limit of 50 pM DNA (estimated from the derived calibration curve, >3 standard deviations). In comparison with the GO-free CPE-based sensor, whose detection limit was 2 nM DNA (Figure S5, Supporting Information), the sensitivity of this GO−**P2** hybrid system was increased by 40-fold.

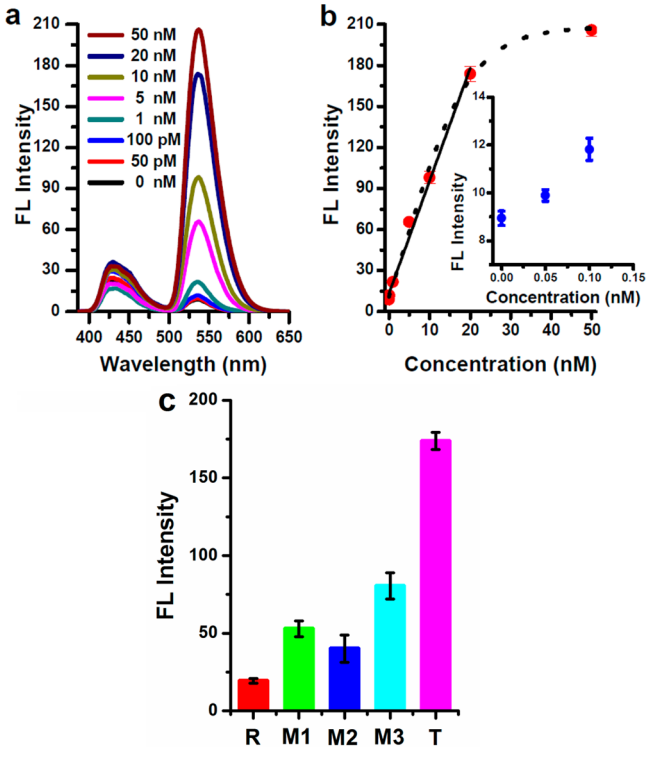

Figure 6. (a) FRET fluorescence spectra of the GO−**P2** system responding to various concentrations of target DNA (**T**: 0−50 nM). (b) Linear relationship between FL intensities and DNA concentrations. Inset: FL intensities at 0, 50, and 100 pM **T**, respectively. (c) The differentiation of a single mismatched sequence with GO−**P2**.

Importantly, our GO−**P2** hybrid system-based DNA detection platform exhibited high specificity. Here, the single mismatched DNA detection was investigated, in which "C" was mismatched by T, A, and G in the middle of target sequence. We found that the single mismatch could be well distinguished from complementary DNA (Figure 6c), indicating our DNA detection possessed the capability of single-nucleotide polymorphisms (SNPs) analysis.

We further generalized our GO−**P2** hybrid detection platform to the analysis of RNA. RNA, especially noncoding RNA, plays critical functions in many biological processes such as cell differentiation and cell apoptosis.[39−41] The variation including insertion and deletion generally leads to the occurrence and development of various kinds of diseases. Recently, microRNAs proved to be highly correlated to cancers, which could be found in serum.[42−45] Therefore, microRNAs are very important in cancer development and have become potential biomarkers for early cancer diagnostic and prognostic prediction. Here, the microRNA of miR141 was introduced to testify the performance of our detection platform in RNA detection. The abnormal expression of miR141 has proved to be highly related to the development of various kinds of cancer.[46,47] We attempted to detect miR141 with our design. Here, the FAM-labled **ssDNA2**, 5′-FAM-CCA TCT TTA CCA GAC AGT GTT A-3′, was used to probe the target miR141 sequence. The results demonstrated that the fluorescence changed with the increase of RNA concentrations (Figure 7a,b). This DNA sensor had a linear range of 0−20 nM, with a detection limit of 50 pM miR141 (estimated from the derived calibration curve, >3 standard deviations). Those data indicated that our detection platform had similar performance for DNA and RNA detection. We also investigated whether this sensor could discriminate miR141 from the mixture of miR141 and total RNA, in which the total RNA was extracted from the blood of a normal adult. Figure 7c illustrated that the extracted total RNA almost could not generate fluorescence change, and the complex of 20 nM miR141 and total RNA had a similar fluorescence with 20 nM miR141.

CONCLUSION

In summary, we have investigated the interaction of different CPEs and GO through the fluorescence quenching of CPEs in the presence of GO. We found that the molecular structure of CPEs, including the main chain and side chain, together with the charge distribution, were highly related to the adsorption of CPEs on GO. We concluded that the charge was the dominant factor for the GO−CPEs interaction. Since GO was negatively charged according to the presence of −COOH and −OH, the CPE with a negative charge exhibited a very weak GO−CPEs interaction. On the other hand, the positively charged CPEs possess a strong interaction with GO, which led to the highly efficient fluorescence quenching. In addition, the conjugated structure of the main chain also contributed to the GO−CPEs interaction, and the conjugated structure tended to adsorb on GO through $\pi-\pi$ interactions. The unique cation−π bonding was the supplementary force for the GO−CPEs interaction due to the characteristic ring structure of GO and cation of CPEs.

DOI: 10.1021/ac504658a
Anal. Chem. 2015, 87, 3877−3883

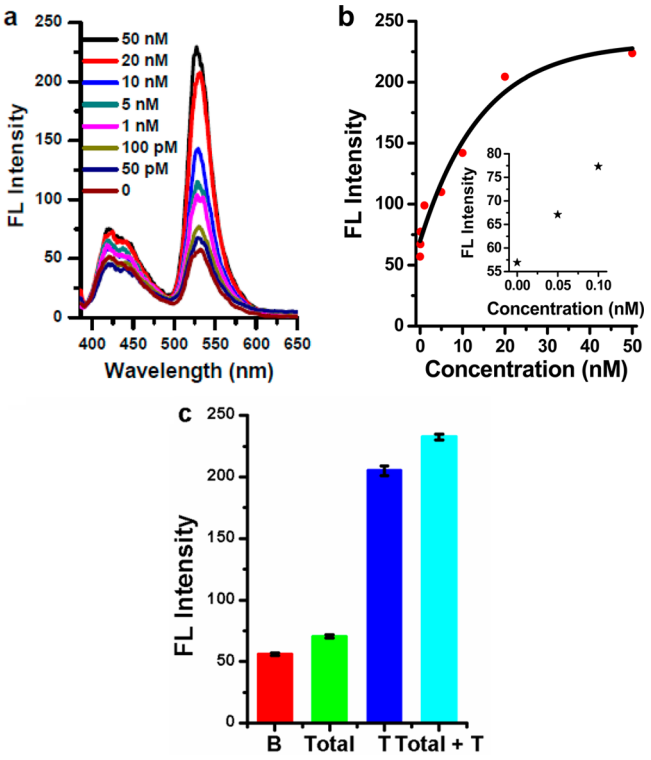

Figure 7. (a) FRET fluorescence spectra of the GO−**P2** system responding to various concentrations of miR141 (0−50 nM). (b) Linear relationship between FL intensities and miR141 concentrations. Inset: FL intensities at 0, 50, and 100 pM miR141, respectively. (c) The fluorescence intensity of miR141 in the absence and presence of the total RNA.

On the basis of the understanding the GO/CPE interaction, we have developed a sensitive homogeneous sensor for DNA and RNA detection. We found the GO−**P2** hybrid system exhibited excellent discrimination of ssDNA and dsDNA, which formed the basis of a novel fluorescent biosensor. It greatly improved the S/N ratio by 18-fold through inhibiting the background signal, thus leading to the high sensitivity and high specificity. This sensor exhibited high performance in DNA and RNA detection, and it presented a detection limit of 50 pM DNA and RNA, about 40-fold that of the GO-free CPE-based sensor (2 nM). The addition of interference materials, such as total RNA, in target solution could not disturb the selective determination of target. This GO−CPE-based sensing strategy possesses great potential in other biosensor systems based on aptamers, proteins, peptides, and other biological probes.

■ ASSOCIATED CONTENT

Supporting Information

Some supplementary spectra data. This material is available free of charge via the Internet at http://pubs.acs.org.

■ AUTHOR INFORMATION

Corresponding Author

*E-mail: wanglihua@sinap.ac.cn.

Author Contributions

†F.L. and J.C. contributed equally.

Notes

The authors declare no competing financial interest.

■ ACKNOWLEDGMENTS

We thank the National Natural Science Foundation of China (21227804, 21390414, and 31371015), the National Basic Research Program of China (973 program, 2013CB932803), Singapore Ministry of Defense (R 279-000-340-232), and the Youth Innovation Promotion Association, CAS, for financial support.

■ REFERENCES

(1) Thomas, S. W.; Joly, G. D.; Swager, T. M. *Chem. Rev.* **2007**, *107*, 1339−1386.
(2) Liu, B.; Bazan, G. C. *J. Am. Chem. Soc.* **2004**, *126*, 1942−1943.
(3) Zhu, C. L.; Liu, L. B.; Yang, Q.; Lv, F. T.; Wang, S. *Chem. Rev.* **2012**, *112*, 4687−4735.
(4) Gaylord, B. S.; Heeger, A. J.; Bazan, G. C. *J. Am. Chem. Soc.* **2003**, *125*, 896−900.
(5) Bout, D. A. V.; Yip, W.-T.; Hu, D.; Fu, D.-K.; Swager, T. M.; Barbara, P. F. *Science* **1997**, *277*, 1074−1077.
(6) Feng, F. D.; He, F.; An, L. L.; Wang, S.; Li, Y. L.; Zhu, D. B. *Adv. Mater.* **2008**, *20*, 2959−2964.
(7) Liu, X. F.; Tang, Y. L.; Wang, L. H.; Zhang, J.; Song, S. P.; Fan, C. H.; Wang, S. *Adv. Mater.* **2007**, *19*, 1471−1474.
(8) Li, C.; Numata, M.; Takeuchi, M.; Shinkai, S. *Angew. Chem., Int. Ed.* **2005**, *44*, 6371−6374.
(9) Duan, X. R.; Li, Z. P.; He, F.; Wang, S. *J. Am. Chem. Soc.* **2007**, *129*, 4154−4155.
(10) He, F.; Tang, Y. L.; Wang, S.; Li, Y. L.; Zhu, D. B. *J. Am. Chem. Soc.* **2005**, *127*, 12343−12346.
(11) Wang, S.; Gaylord, B. S.; Bazan, G. C. *J. Am. Chem. Soc.* **2004**, *126*, 5446−5451.
(12) Feng, F. D.; Liu, L. B.; Wang, S. *Nat. Protoc.* **2010**, *5*, 1255−1264.
(13) Miranda, O. R.; You, C. C.; Phillips, R.; Kim, I. B.; Ghosh, P. S.; Bunz, U. H. F.; Rotello, V. M. *J. Am. Chem. Soc.* **2007**, *129*, 9856−9857.
(14) Ho, H. A.; Boissinot, M.; Bergeron, M. G.; Corbeil, G.; Doré, K.; Boudreau, D.; Leclerc, M. *Angew. Chem., Int. Ed.* **2002**, *114*, 1618−1621.
(15) Liu, B.; Bazan, G. C. *Chem. Mater.* **2004**, *16*, 4467−4476.
(16) Zheng, B.; Wang, C.; Wu, C. Y.; Zhou, X. J.; Lin, M.; Wu, X. C.; Xin, X.; Chen, X.; Xu, L.; Liu, H.; Zheng, J.; Zhang, J. Y.; Guo, S. W. *J. Phys. Chem. C* **2012**, *116*, 15839−15846.
(17) Balapanuru, J.; Yang, J. X.; Xiao, S.; Bao, Q. L.; Jahan, M.; Polavarapu, L.; Wei, J.; Xu, Q. H.; Loh, K. P. *Angew. Chem., Int. Ed.* **2010**, *49*, 6549−6553.
(18) Wang, L. H.; Pu, K.-Y.; Li, J.; Qi, X. Y.; Li, H.; Zhang, H.; Fan, C. H.; Liu, B. *Adv. Mater.* **2011**, *23*, 4386−4391.
(19) He, S. J.; Song, B.; Li, D.; Zhu, C. F.; Qi, W. P.; Wen, Y. Q.; Wang, L. H.; Song, S. P.; Fang, H. P.; Fan, C. H. *Adv. Funct. Mater.* **2010**, *20*, 453−459.
(20) Feng, B. Y.; Guo, L. J.; Wang, L. H.; Li, F.; Lu, J. X.; Gao, J. M.; Fan, C. H.; Huang, Q. *Anal. Chem.* **2013**, *85*, 7732−7737.
(21) Xing, X. J.; Liu, X. G.; He, Y.; Lin, Y.; Zhang, C. L.; Tang, H. W.; Pang, D. W. *Biomacromolecules* **2012**, *14*, 117−123.
(22) Ho, H. A.; Leclerc, M. *J. Am. Chem. Soc.* **2004**, *126*, 1384−1387.
(23) Ho, H. A.; Béra-Abérem, M.; Leclerc, M. *Chem.—Eur. J.* **2005**, *11*, 1718−1724.
(24) Pu, K. Y.; Liu, B. In *Advanced Fluorescence Reporters in Chemistry and Biology II: Molecular Constructions, Polymers and Nanoparticles*; Springer-Verlag: Berlin Heidelberg, 2010; Vol. *9*, pp 417−454.
(25) Huang, F.; Wang, X. H.; Wang, D. L.; Yang, W.; Cao, Y. *Polymer* **2005**, *46*, 12010−12015.
(26) Ho, H. A.; Boissinot, M.; Bergeron, M. G.; Corbeil, G.; Dore, K.; Boudreau, D.; Leclerc, M. *Angew. Chem., Int. Ed.* **2002**, *41*, 1548−1551.
(27) Dreyer, D. R.; Park, S.; Bielawski, C. W.; Ruoff, R. S. *Chem. Soc. Rev.* **2010**, *39*, 228−240.

DOI: 10.1021/ac504658a
Anal. Chem. 2015, 87, 3877−3883

(28) Dreyer, D. R.; Todd, A. D.; Bielawski, C. W. *Chem. Soc. Rev.* **2014**, *43*, 5288−5301.
(29) Varghese, N.; Mogera, U.; Govindaraj, A.; Das, A.; Maiti, P. K.; Sood, A. K.; Rao, C. N. R. *ChemPhysChem* **2009**, *10*, 206−210.
(30) Bout, D. A. V.; Yip, W.-T.; Hu, D.; Fu, D.-K.; Swager, T. M.; Barbara, P. F. *Science* **1997**, *277*, 1074−1077.
(31) Li, F.; Pei, H.; Wang, L. H.; Lu, J. X.; Gao, J. M.; Jiang, B. W.; Zhao, X. C.; Fan, C. H. *Adv. Funct. Mater.* **2013**, *23*, 4140−4148.
(32) Li, J.; Huang, Y.; Wang, D. F.; Song, B.; Li, Z. H.; Song, S. P.; Wang, L. H.; Jiang, B. W.; Zhao, X. C.; Yan, J.; Liu, R.; He, D. N.; Fan, C. H. *Chem. Commun.* **2013**, *49*, 3125−3127.
(33) Liu, J. W. *Phys. Chem. Chem. Phys.* **2012**, *14*, 10485−10496.
(34) Hassan, M.; Walter, M.; Moseler, M. *Phys. Chem. Chem. Phys.* **2014**, *16*, 33−37.
(35) McGaughey, G. B.; Gagné, M.; Rappé, A. K. *J. Biol. Chem.* **1998**, *273*, 15458−15463.
(36) Gao, Y.; Li, Y.; Zhang, L.; Huang, H.; Hu, J. J.; Shah, S. M.; Su, X. *J. Colloid Interface Sci.* **2012**, *368*, 540−546.
(37) Solvent Miscibility and Viscosity Chart. Adapted from *The HPLC Solvent Guide*; Sadek, P.; Wiley-Interscience: Hoboken, NJ, 2002.
(38) Lu, C. H.; Yang, H. H.; Zhu, C. L.; Chen, X.; Chen, G. N. *Angew. Chem., Int. Ed.* **2009**, *121*, 4879−4881.
(39) Lu, J.; Getz, G.; Miska, E. A.; Alvarez-Saavedra, E.; Lamb, J.; Peck, D.; Sweet-Cordero, A.; Ebet, B. L.; Mak, R. H.; Ferrando, A. A.; Downing, J. R.; Jacks, T.; Horvitz, H. R.; Golub, T. R. *Nature* **2005**, *435*, 834−838.
(40) Pritchard, C. C.; Cheng, H. H.; Tewari, M. *Nat. Rev. Genet.* **2012**, *13*, 358−369.
(41) Bartel, D. P. *Cell* **2004**, *116*, 281−297.
(42) Mitchell, P. S.; Parkin, R. K.; Kroh, E. M.; Fritz, B. R.; Wyman, S. K.; Pogosova-Agadjanyan, E. L.; Peterson, A.; Noteboom, J.; O'Briant, K. C.; Allen, A.; Lin, D. W.; Urban, N.; Drescher, C. W.; Knudsen, B. S.; Stirewalt, D. L.; Gentleman, R.; Vessella, R. L.; Nelson, P. S.; Martin, D. B.; Tewari, M. *Proc. Natl. Acad. Sci. U. S. A.* **2008**, *105*, 10513−10518.
(43) Brase, J. C.; Wuttig, D.; Kuner, R.; Sueltmann, H. *Mol. Cancer* **2010**, *9*, 306.
(44) Song, M. Y.; Pan, K. F.; Su, H. J.; Zhang, L.; Ma, J. L.; Li, J. Y.; Yuasa, Y.; Kang, D.; Kim, Y. S.; You, W. C. *PLoS One* **2012**, *7*, No. e33608.
(45) Zheng, D. L.; Haddadin, S.; Wang, Y.; Gu, L. Q.; Perry, M. C.; Freter, C. E.; Wang, M. X. *Int. J. Clin. Exp. Pathol.* **2011**, *4*, 575−586.
(46) Cheng, H.; Zhang, L.; Cogdell, D. E.; Zheng, H.; Schetter, A. J.; Nykter, M.; Harris, C. C.; Chen, K.; Hamilton, S. R.; Zhang, W. *PLoS One* **2011**, *6*, No. e17745.
(47) Zhao, G.; Wang, B.; Liu, Y.; Zhang, J. G.; Deng, S. C.; Qin, Q.; Tian, K.; Li, X.; Zhu, S.; Niu, Y.; Gong, Q.; Wang, C. Y. *Mol. Cancer Ther.* **2013**, *12*, 2569−2580.

DOI: 10.1021/ac504658a
Anal. Chem. 2015, 87, 3877−3883